Title

Force Feedback Controls Motor Activity and Mechanical Properties of Self-Assembling Branched Actin Networks.

Journal

Cell, 164(1-2)

ISSN

0092-8674

Authors

Bieling, Peter
Li, Tai-De
Weichsel, Julian
et al.

Publication Date

2016

DOI

10.1016/j.cell.2015.11.057

Peer reviewed

HHS Public Access

Author manuscript

Cell. Author manuscript; available in PMC 2017 January 14.

Published in final edited form as:

Cell. 2016 January 14; 164(1-2): 115–127. doi:10.1016/j.cell.2015.11.057.

Force feedback controls motor activity and mechanical properties of self-assembling branched actin networks

Peter Bieling[1,2,*], **Tai-De Li**[2,3,4,*], **Julian Weichsel**[5], **Ryan McGorty**[6], **Pamela Jreij**[2], **Bo Huang**[6], **Daniel A. Fletcher**[2,3,†], and **R. Dyche Mullins**[1,†]

[1]Department of Cellular and Molecular Pharmacology and Howard Hughes Medical Institute, University of California, San Francisco, Genentech Hall, 600 16th St., San Francisco, CA 94158, USA

[2]Department of Bioengineering & Biophysics Program, University of California, Berkeley, 648 Stanley Hall MC 1762, Berkeley, CA 94720, USA

[3]Physical Biosciences Division, Lawrence Berkeley National Laboratory, 648 Stanley Hall MC 1762, Berkeley, CA 94720, USA

[4]Advance Science Research Center, City University of New York, 85 St Nicholas Terrace, NY 10031, USA

[5]Department of Chemistry, University of California, Berkeley, 207 Gilman Hall, Berkeley, CA 94720, USA

[6]Department of Biochemistry and Biophysics, University of California, San Francisco, Genentech Hall, 600 16th St., San Francisco, CA 94158, USA

Abstract

Branched actin networks–created by the Arp2/3 complex, capping protein, and a nucleation promoting factor– generate and transmit forces required for many cellular processes, but their response to force is poorly understood. To address this, we assembled branched actin networks *in vitro* from purified components and used simultaneous fluorescence and atomic force microscopy to quantify their molecular composition and material properties under various forces. Remarkably, mechanical loading of these self-assembling materials increases their density, power, and efficiency. Microscopically, increased density reflects increased filament number and altered geometry, but no change in average length. Macroscopically, increased density enhances network stiffness and resistance to mechanical failure beyond those of isotropic actin networks. These

[†]corresponding authors: order of listing determined by coin toss. fletch@berkeley.edu, Dyche.Mullins@ucsf.edu.
[*]equal contribution

Author Contributions

P.B. and T.-D.L. designed and performed experiments and wrote the manuscript. P.B. purified the proteins and analyzed fluorescence data. T.-D.L. developed the AFMs and analyzed mechanical data. P.B., T.-D.L., and P.J. developed the biochemical surface micro-patterning. J.W. developed software for the analysis of single molecule data. R.M and B.H. designed and built the 3D-STORM and R.M analyzed STORM data. D.A.F. and R.D.M. supervised the project and wrote the manuscript.

effects endow branched actin networks with memory of their mechanical history that shapes their material properties and motor activity. This work reveals intrinsic force feedback mechanisms by which mechanical resistance makes self-assembling actin networks stiffer, stronger, and more powerful.

Introduction

Cells are physical objects that interact with the world around them by generating, transmitting, and resisting forces (Janmey and McCulloch, 2007; Kasza et al., 2007). In eukaryotic cells many of these forces flow through the collection of cross-linked, branched, and entangled filament networks that form the actin cytoskeleton (Fletcher and Mullins, 2010; Pollard and Cooper, 2009). Branched actin networks, for example, generate pushing forces (Mogilner and Oster, 1996) required for many cellular processes, including: protrusion of leading edge membranes in migrating cells (Bisi et al., 2013; Wu et al., 2012), motility of intracellular pathogens (Welch and Way, 2013), healing of cell ruptures (Clark et al., 2009), endocytosis (Mooren et al., 2012), phagocytosis (Insall and Machesky, 2009), and the formation of tight cell adhesions (Yamaguchi et al., 2005). These dynamic actin networks are created by the branching activity of the Arp2/3 complex, which creates new filaments from the sides of preexisting filaments (Mullins et al., 1998). In addition to the Arp2/3 complex, assembly of force-generating networks requires two accessory proteins: a WASP-family nucleation promoting factor (NPF) and a filament capping protein (Akin and Mullins, 2008). Despite the mechanical nature of their functions we know little about how branched actin networks respond to force at the molecular or the material level (Chaudhuri et al., 2007; Marcy et al., 2004; Parekh et al., 2005; Pujol et al., 2012). Previous work focused on mechanics of isotropic actin networks held together by entanglement or cross-linking (Stricker et al., 2010), which are dominated by “entropic elasticity” of individual actin filaments (Gardel et al., 2004a; MacKintosh et al., 1995; Storm et al., 2005; Wagner et al., 2006). Theory developed from this work explains effects of “pre-stress” on actin gels (Gardel et al., 2006), but its connection to the dynamic and anisotropic cytoskeletal networks created by living cells remains unclear.

Cells construct actin networks by concentrating assembly factors at specific sites, establishing physical boundary conditions that dictate dynamics and architecture of the network. Filament nucleation and branching by the Arp2/3 complex, for example, creates actin networks that generate force to drive membrane movement (Svitkina and Borisy, 1999; Vinzenz et al., 2012; Wu et al., 2012). Because Arp2/3 activity depends on membrane-associated NPFs, new filaments are created only in a narrow zone adjacent to the membrane. Imposing this boundary condition on filament formation produces anisotropic networks in which most growing filament ends point toward the membrane (Maly and Borisy, 2001; Weichsel et al., 2012) and has profound mechanical consequences. Isotropic networks assembled *in vitro* from soluble and randomly distributed Arp2/3 complexes are mechanically weak (Nakamura et al., 2002), while networks assembled from surface-immobilized NPFs are more coherent and much stiffer (Chaudhuri et al., 2007; Marcy et al., 2004). Once polarized, growing actin networks encounter obstacles and experience external forces that may affect their assembly.

Here, we ask how mechanical forces affect the biochemical interactions that underlie network assembly, and we investigate how the mechanical history of self-assembling networks affects their material properties and motor activity. To measure molecular and mechanical responses of branched actin networks to force, we applied simultaneous Total Internal Reflection Fluorescence (TIRF) and Atomic Force Microscopy (AFM) to actin networks assembled from purified components. To create biologically relevant boundary conditions for network growth we micro-patterned the surface of glass coverslips with a WASP-family NPF. We then quantified incorporation of proteins into growing networks by TIRF microscopy. At the same time, we used an AFM cantilever to apply force and quantify network growth velocity. To understand the functional consequences of biochemical responses to force, we also used the AFM cantilever to measure material properties of branched actin networks grown under different physical and biochemical conditions.

We find that force fundamentally alters the assembly, architecture, and function of branched actin networks: growth velocity *decreases* while filament density *increases* in response to force. Microscopically, the increase in filament density reflects two changes: (i) greater number of pushing filaments and (ii) tighter filament packing. Average filament length, however, does not change with force. Interestingly, the fractional energy of polymerization converted into mechanical work increases with applied force. Macroscopically, force on growing actin networks enhances their stiffness and mechanical resilience. Networks exhibit their maximum stiffness when loaded with the same forces they experienced during growth. These force-induced changes in material properties, however, do not scale with density or stress according to “universal” laws derived for isotropic actin gels (Gardel et al., 2004b, 2006). This argues that the physics of Arp2/3-generated actin networks differs fundamentally from that of random, cross-linked networks. Furthermore, we find that assembling branched actin networks under changing load forces produces materials whose stiffness and force-velocity relationships are dominated by their loading history rather than molecular composition.

Results

Assembly of branched actin networks with physiologically relevant boundary conditions

To mimic enrichment of WASP-family NPFs on cellular membranes, we immobilized the Arp2/3-activating region of WAVE1 on functionalized coverslips ((Fourniol et al., 2014); Fig. 1A). We then added purified components —monomeric actin, Arp2/3 complex, and capping protein (CP) — to the WAVE1ΔN patterns to create polarized actin networks. To prevent spontaneous nucleation, we also added the actin-binding protein profilin (Pantaloni and Carlier, 1993; Tilney et al., 1983). By confocal fluorescence microscopy networks formed 3-dimensional ‘pillars’ growing from WAVE1ΔN-coated squares (Fig. 1B) at 7.33 ± 1.61 μm/min (Suppl. Fig. 1A), at rates comparable to actin assembly at the leading edge of migrating cells (Renkawitz et al., 2009). Growth velocity did not strongly depend on NPF pattern size, indicating that network assembly is not limited by diffusion (Suppl. Fig. 1B). Because less than 0.01% of the coverslip is coated with the NPF, network growth did not significantly deplete the pool of soluble protein components and the filament networks grew with constant density and velocity for more than an hour (Suppl. Fig. 1C). The distribution

of fluorescent Arp2/3 (not shown) and CP (Fig. 1C,D) were also homogeneous throughout the networks.

We used TIRF microscopy to quantify the rate at which individual molecules of actin, CP and Arp2/3 join the growing network at the NPF-coated surface. We reduced the fraction of labeled actin to 1 in $1.5x10^6$ molecules, which enabled us to visualize incorporation of individual actin monomers into the network. Each incorporation event was marked by the sudden appearance of a fluorescent spot within an NPF square (Fig. 1E, top panel) that subsequently decayed exponentially with time as the molecule moved with the growing network out of the evanescent excitation field (Fig. 1E, Suppl. Fig. 1D, Suppl. Movie 1, Suppl. Methods). We counted single-molecule binding events and then divided their frequency by the actin labeling ratio to compute a total polymerization rate of 7135 actin monomers-$sec^{-1}\mu m^{-2}$ under our experimental conditions.

Using this single-molecule approach we also determined the total rates of nucleation/branching (68 Arp2/3 -$sec^{-1}\mu m^{-2}$) and capping (57 CP-$sec^{-1}\mu m^{-2}$; Fig. 1E, middle and bottom). The similarity of these rates indicates that most growing filament ends generated by NPF-stimulated Arp2/3 activity at the coverslip surface are also capped near this surface, within the shallow TIRF illumination field. We calculated the average filament length in two ways: by the ratio of polymerization rate to the rate of nucleation or capping (Fig. 1F) and found that our filaments grew to a mean length of about 300 nm (or 110 monomers), similar to filament lengths observed in branched networks *in vivo* (Vinzenz et al., 2012). We conclude that our reconstituted system captures the basic architecture and assembly dynamics of cellular actin networks.

Effect of load on branched actin network velocity, density, and efficiency

To measure network growth and to apply compressive forces, we positioned an AFM cantilever over an NPF-coated square before initiating network assembly (Fig. 2A). To apply constant force to a growing network, we used optical feedback to maintain constant deflection of the AFM cantilever. We divide the cantilever force by the cross-sectional area of the actin network (200 μm^2) and report our measurements as force per unit area or stress ($pN/\mu m^2$ or equivalently, Pa). We first applied a stepwise series of increasing load forces to a growing network and measured steady-state growth velocity after the network adapted to the new growth force (Suppl. Fig. 2). This steady-state growth velocity fell sharply under small loads (Fig. 2B) but did not stall completely until the load exceeded 1250 $pN/\mu m^2$, a value comparable to pushing and pulling stresses generated by crawling cells (Gardel et al., 2008; Prass et al., 2006). The new steady-state growth velocity did not depend on previous forces (Suppl. Fig. 3), indicating that instantaneous force alone determines network growth at steady-state. Finally, the force velocity curve does not follow a simple exponential decay as expected for a fixed number of growing filaments by Elastic Brownian Ratchet models (Peskin et al., 1993). Instead, velocity falls sharply at low force but decreases more gradually at higher force (Fig. 2B), suggesting a possible load-dependent effect on filament density.

To determine the effect of force on filament density, we performed TIRFM of fluorescent actin incorporating into networks growing under load (Fig. 2C). While growth velocity decreases with applied load, the density of actin filaments in the network increases strongly

(Fig. 2D,E, Suppl. Fig. 3, Suppl. Movie 2). This increased filament density does not reflect elastic compression but rather stable, force-induced changes in the material (see next section). The fall in growth velocity and the rise in filament density nearly compensate each other, adding up to a surprisingly weak, load-dependent decrease in the rate of actin incorporation (flux) into the network (Fig. 2F). Using our single-molecule measurement of actin polymerization under low growth force (Fig. 1E) as calibration, we calculated assembly rates and filament densities for networks grown under other loading conditions (right y-axes, Fig. 2F,E). Over the functional force range —from zero load to network stall —filament concentration in the network increases from 0.125 mM to 1 mM (filament volume fractions of 0.5 – 3.7 %).

From basic thermodynamics (Hill and Kirschner, 1982), we estimated the free energy change of one actin monomer adding to the barbed end of a filament under our experimental conditions (Suppl. Methods). Multiplying this value by the actin flux yields the rate of energy consumption by the network as it pushes against various loads (Fig. 2G). We used the force-velocity relationship of our branched networks (Fig. 2B) to calculate the mechanical power output (product of force and growth velocity) at each force (Fig. 2G). The ratio of the power output to the energy consumption rate yields the efficiency of the branched actin network as a motor (Fig. 2H). This efficiency turns out to be highly load-dependent, increasing from ~3% at low force to about ~14% at high force. Thus, polymerizing filaments appear to share their burden more evenly under high load, with fewer futile polymerization events occurring away from the network/load boundary.

Architecture and assembly kinetics of branched networks adapt to load

We find that force increases filament density in branched actin networks, but does this reflect: (a) more polymerizing filaments; (b) a shift in network microstructure to denser packing; or (c) both (Fig. 3A)? To determine whether load increases the number of polymerizing filaments, we developed an ‘arrest-and-label’ method to visualize free filament ends in the network (Suppl. Fig. 4). Briefly, we assembled two dendritic networks side-by-side: one unloaded and one growing against defined load. We then arrested network assembly by adding Phalloidin and Latrunculin B, together with a fluorescent derivative of CP (Fig. 3B). The two small-molecules rapidly freeze actin dynamics (Akin and Mullins, 2008), while the fluorescent CP labels free barbed ends of filaments in the network (Fig. 3B, Suppl. Fig. 4, Suppl. Movie 3). Accumulation of labeled CP was biphasic (Suppl. Fig. 4D,E, Suppl. Methods), with rapid binding to free barbed ends followed by a very slow exchange of labeled CP with unlabeled CP throughout the network (Reymann et al., 2011; Schafer et al., 1996). In addition to TIRFM, we used 3-dimensional stochastic optical reconstruction microscopy (3D-STORM, (Huang et al., 2008); Suppl. Methods) to count free barbed ends in the network. The use of 3D-STORM enabled us to rule out potential TIRF artifacts, such as compression of free ends into the evanescent field (Suppl. Fig. 5). Both TIRF and 3D-STORM imaging of fluorescent CP after growth arrest showed that the number of free barbed ends in the dendritic network increases strongly (~3.3-fold) with force (Fig. 3C).

To estimate the absolute number of free barbed ends, we combined these data with single-molecule measurements of actin incorporation. Based on the growth velocity of our

networks under low force (7.33 μm/min, Suppl. Fig. 1), we estimate one free barbed end incorporates ~46 monomers per second, which implies the existence of ~160 growing filament ends/μm^2 under low force. This number increases to ~550/μm^2 at high load forces near stall. If growing barbed ends share this load equally, then each polymerizing filament generates 1.9 pN of force under high loads. This greater number of growing filaments only partly accounts for the observed increase in filament density under load (Fig. 3D), suggesting that micro-structural changes also occur in the network.

Since force causes changes in filament number and geometry we looked for other force-induced effects on network architecture, including changes in filament length. As above, we calculated average filament length in two ways, from the ratio of fluorescent Arp2/3 complex (on pointed ends) and CP (on barbed ends) to polymeric actin in the network (Fig. 3F), which we calibrated with our single-molecule measurmements of CP, Arp2/3 complex, and actin incorporating into networks under low force (Fig. 1E,F). Remarkably, theses measurements reveal that the mean filament length in a branched actin network remains constant from low loads that have little effect on network growth up to high loads that almost cause them to stall (Fig. 3F). These results suggest that robustness of network stoichiometry under load reflects a close match between the force responses of filament elongation and capping.

Mechanics of branched actin networks depends on the force experienced during growth

How do load-induced changes in network architecture affect the ability of branched networks to transmit and resist forces? To address this question, we used AFM-based micro-rheometry to probe the material properties of branched actin networks grown under various loads (Fig. 4A). We assembled networks under a constant *growth force* and arrested their assembly at a height of 10 μm with Latrunculin B. The slow dissociation of CP (Schafer et al., 1996) and the Arp2/3 complex (Beltzner and Pollard, 2008) from branched filaments ensured that networks remain essentially constant during the time required to measure their material properties (see Suppl. Fig. 6A, Methods). After assembly under load and kinetic arrest, we performed AFM micro-rheometry on networks at a small, constant force (12.5–25 pN/μm^2). Under these “relaxed” conditions we measured elasticity in the range of 10^3–10^4 Pa, consistent with previous measurements on branched networks (Chaudhuri et al., 2007; Marcy et al., 2004; Pujol et al., 2012) (Fig. 4B). Both the elastic (Fig. 4B) and viscous moduli (Suppl. Fig. 6C) increased with increasing growth force, a change that corresponded to increased filament density. Interestingly, when we removed the growth force immediately following arrest, the height of the network increased only slightly (10%, Fig. 4C), regardless of the magnitude of the force. This minimal height change shows that force-dependent increases in actin density are stored in the microarchitecture of the network and are not the result of elastic compression.

Branched actin networks are maximally elastic and minimally viscous under loads that match their original growth force

Many biological polymer networks assembled in the absence of force exhibit strong stiffening when subjected to subsequent loads or “pre-stress” (Gardel et al., 2006; Janmey et al., 1991; Storm et al., 2005). To investigate the mechanical response of branched networks,

we performed rheology measurements on growth-arrested actin networks assembled at various growth forces and subsequently pre-stressed with a range of 'test loads' (Fig. 4D, Suppl. Fig. 7). We find that branched actin networks are stiffest when the *test load* matches the original *growth force* experienced during its assembly. When tested at loads above or below the original growth force, the material either becomes softer or remains the same (Fig. 4E). Sparse networks assembled at low growth forces exhibit little softening at lower test loads, while denser networks assembled under high growth forces soften more significantly (4-fold) (Fig. 4E). Similarly, when loaded beyond the growth force, the stiffness of sparse networks remained relatively constant, while dense networks softened. To better compare the behavior of branched networks assembled at different growth forces, we normalized the applied test load by the original growth force. We also normalized the elasticity measured under high test-loads by the initial elasticity of the 'relaxed' material. The normalized data illustrate that maximum stiffness occurs when the test load equals the growth force (Fig. 4F). Interestingly, the viscous modulus of branched actin networks falls to a minimum when the test load equals the growth force, and increases at lower and higher test loads (Fig. 4G,H). These data reveal that growing branched actin networks adapt to a specific growth force to become maximally stiff and minimally viscous at that load.

Loading branched networks beyond their growth force results in mechanical failure

We next measured recovery of the height of self-assembled actin networks following release of a test load (Fig. 5A). Purely elastic materials recover 100% of their original height after force release, but we found that branched actin networks show load-dependent, irreversible height loss following high loads (Fig. 5B). Such irreversible plastic deformation is analogous to crushing of a material such as Styrofoam, and usually reflects permanent micro-structural changes in the material. Networks assembled under high growth forces are stiffer and more resilient to deformation compared to networks grown under low load. Normalizing the test load by the growth force causes all of our deformation data to collapse onto a single curve (Fig. 5C), and reveals that the growth force also defines a critical point beyond which the material irreversibly changes. Structural failure was also evident when we measured network elasticity. When subjected to test loads below the growth force, network stiffness recovered to nearly its original value upon test load release. Once loading exceeded the growth force, however, the network failed to recover its original elasticity (Fig. 5D,E). Such irreversible changes could affect the growth rate and elastic properties of branched actin networks exposed to varying physical boundary conditions.

Time-varying forces create inhomogeneous actin networks with composite properties

In vivo actin networks experience changing forces in a complex and heterogeneous environment. Applying such time-varying forces to growing actin networks yields inhomogeneous materials, with layers of different filament density. To study such inhomogeneous materials we assembled branched networks under changing growth forces, arrested their assembly, and measured their elasticity under varying test loads. To create two-layered networks we first assembled a dense network under 500 pN/μm^2 (Fig. 5F, left). At a height of 4 μm, we reduced the load to 25 pN/μm^2 (Fig. 5F, right) and assembled an additional 6 μm of sparser network. We compared the mechanics of this bi-layered material to homogeneous networks assembled under high or low force alone (Fig. 5G). If the bi-

layered network was purely elastic its stiffness would be dominated by the weaker material (Fig. 5G, dashed magenta line, Suppl. Methods). Instead, as the test load approached the higher growth force, we observed stiffening in the inhomogeneous material that was intermediate between those of the high- and low-density materials (Fig. 5G, middle green line). This result is explained entirely by plastic deformation of the low-density layer when test load exceeds its growth force (Fig. 5G, solid magenta line; Suppl. Methods). Once the weaker layer is crushed, the properties of the composite shift toward those of the denser material. In this way, mechanical failure may enable inhomogeneous actin networks to adapt more quickly to high load forces.

Anisotropic, branched actin networks behave differently than isotropic, crosslinked networks

The stiffness of random, isotropic actin networks (both cross-linked or entangled) scales roughly as the square of filament density (Fig. 6A, Gardel et al., 2003). We wondered whether the same characteristic power-law scaling of stiffness with density describes anisotropic, branched actin networks assembled under load. Comparing our results with published data, we find that branched networks generated by localized activity of the Arp2/3 complex are much denser and stiffer than isotropic actin networks (Fig. 6A). Their elastic modulus, however, scales much more weakly with filament density ($\sim c_A 0.6$, where c_A is the concentration of filamentous actin). Previous studies have also suggested that stress-induced stiffening of isotropic actin networks follows a ‘universal’ power law, in which the elastic modulus increases as the ~1.5 power of the “pre-stress”. We find that, while branched actin networks exhibit stress-stiffening, this behavior does not match that of isotropic networks and does not follow a single power law across all network densities. Moreover, we observe branched network stiffening at forces more than an order of magnitude beyond the point of isotropic network failure (Fig. 6B). The physics of branched actin networks, therefore, appears to be distinct from random gels.

Filament crosslinking proteins stiffen branched actin networks but do not shift the critical force that defines their material properties

Actin filament crosslinkers Filamin-A and α-Actinin are thought to strengthen some branched actin networks *in vivo* (Flanagan et al., 2001; Vinzenz et al., 2012). We investigated the effect of these crosslinkers by growing branched actin networks under constant force, terminating their growth with Latrunculin B, and then adding either Filamin-A or α-Actinin. By visualizing labeled crosslinkers with confocal microscopy, we determined the affinities of Filamin-A and α-Actinin for branched actin networks as K_D = 0.37 μM and 2.12 μM, respectively (Fig. 6C), in agreement with previous studies (Nakamura et al., 2007; Wachsstock et al., 1993). Both crosslinkers stiffened branched networks (Fig. 6D), but we observed interesting differences between them (Fig. 6D). Dense actin networks assembled under high forces stiffened more when crosslinked by α-Actinin than by Filamin-A, while sparse networks assembled under low load showed the opposite behavior (Fig. 6D, inset). Neither crosslinker qualitatively changed the shape of the stress-stiffening curve, indicating that the mechanical response of branched actin networks is dominated by their load-adaptive architecture rather than by properties of the crosslinker. Interestingly, Filamin-A and α-Actinin also produced different effects on plastic deformation of branched actin

networks loaded above their growth force. Both crosslinkers protected sparse networks from plastic deformation, but α-Actinin provided less protection than Filamin-A (Fig. 6E). Conversely, both crosslinkers *increased* plastic deformation of denser networks, probably by 'locking in' filament contacts induced by compression. Under these conditions α-Actinin enhanced deformation more than Filamin-A (Fig. 6F).

Motor activity of branched actin networks depends on loading history

What happens when a growing actin network pushes against a material with a defined stiffness rather than against a constant force? The extracellular matrix, for example, can offer defined mechanical resistance to actin-driven pseudopod extension (Fig. 7A). A network growing against a barrier of defined stiffness does not feel constant force, but a steadily increasing force that depends on how far the barrier is displaced. We, therefore, compared the velocities of branched actin networks grown against AFM cantilevers whose deflection was controlled in two different ways. In one experiment, we applied a *constant force* (as before) by moving the cantilever base along with the growing network maintaining constant cantilever deflection (Fig. 7B, left). Under these conditions, force on the network does not depend on network height. In the second experiment, the cantilever base remains stationary and deflection increases as the network grows (Fig. 7B, right). In this mode, the cantilever mimics a Hookean spring or an elastic material with a *constant stiffness*. The more the cantilever is deflected, the more force it exerts. To investigate how network growth responds to changing mechanical constraints we performed two-step experiments. First, we assembled two networks under the same *constant force*. We then switched the two networks to grow against two boundaries of different *constant stiffness*. Interestingly, velocity of the network pushing against the stiffer barrier fell instantly even though force on the network increased gradually and by a small amount over the short time (<15sec) of this experiment (Fig. 7C). Next, we assembled two networks under two different *constant forces*, one high and one low. We then switched both networks to grow against the same *constant stiffness* barrier. In this case, the velocity of the sparse network grown under low force immediately drops below that of the denser network, even though: (i) the sparse network's velocity was initially much greater and (ii) the force the sparse network experiences during the second part of the experiment is much less than that experienced by the denser network (Fig. 7D). This result can be explained by how the free energy of actin filament assembly partitions between cantilever deflection and deformation of the network. In constant stiffness mode, the network and cantilever act as two springs in series. When the cantilever mode switches from *constant force* to *constant stiffness*, the force immediately rises above the critical force of the network (the original growth force) and, therefore, actin assembly begins to both deflect the cantilever and to crush older parts of the network. This partitioning immediately reduces the growth velocity.

To test our understanding of this energy partitioning within the network, we used several known parameters – network elasticity (Fig. 4E), growth velocity under constant force (Fig. 7C,D), and cantilever spring constant, to calculate the growth velocity expected at the moment of switching from *constant force* to *constant stiffness* (Suppl. Methods). These calculated values agree well with measured velocities (dashed lines in Fig. 7C,D) demonstrating how the instantaneous (but not the steady-state) growth velocity of branched

actin networks depends on loading history. This complex dependence manifests in the different height changes of branched networks growing under constant stiffness barriers (Fig. 7E) and in the force-velocity relationships calculated from them (Fig. 7F). The steady-state velocities measured under constant force define the upper bound on growth rates at all forces (Fig. 7F, blue dashed line). In contrast, the steadily increasing forces experienced during growth against an elastic barrier create a time-varying loading history and produce not one but a family of force-velocity relationships that define the “motor activity” of branched actin networks.

Discussion

The present study demonstrates that force plays a major role in defining the architecture, mechanics, and function of branched actin networks. Specifically, we identified an intrinsic force-feedback mechanism by which load forces experienced during self-assembly increase filament density and make growing networks stiffer and more resistant to mechanical failure. Importantly, the change in mechanical properties associated with increased filament density does not obey scaling relationships that describe isotropic crosslinked or entangled actin gels.

Average filament length is invariant under load

Elongation of actin filaments slows dramatically under load, but this slowing has no effect on the average length of filaments in a self-assembling branched network. The reason is that filament capping responds to force in the same way as filament elongation. Individual filaments grow slower under load, but because capping is also slower, they grow for a proportionally longer time, reaching the same length. The force-invariance of filament length has important consequences for the material properties of branched actin networks. If, for example, filament length *decreased* with applied force, the overall coherence of the network would decrease due to loss of entanglement between branched filament arbors. Conversely, a force-induced *increase* in average filament length would produce filaments that buckle more easily under lower forces. Either response would nudge the material properties of the network toward a regime that is *less* capable of resisting the applied load.

Force alters internal architecture of branched actin networks

Over the range from zero load to forces that stall network growth, the filament density of a branched actin network increases by about an order of magnitude. A force-dependent increase in the number of free barbed ends (manuscript in preparation) accounts for part of this increase in density (~3.5-fold), while the remainder (~3 fold) must reflect changes in filament packing. This is most easily visualized in terms of the angle between the filaments and the boundary surface they push against. In the absence of strong forces opposing growth, filaments in branched actin networks *in vivo* (Svitkina and Borisy, 1999; Weichsel et al., 2012), *in vitro* (Cameron et al., 2001) and *in silico* (Maly and Borisy, 2001; Schaus et al., 2007) are distributed symmetrically around an average angle of ~54° with respect to the membrane. This angle of attack is determined primarily by the geometry of ~72° y-branches made by the Arp2/3 complex. A 3-fold increase in filament density could be produced by a 3-fold decrease in the sine of the average angle of attack: from ~54° to ~16°. This shallower

angle of attack could be produced by bending filaments or branch-points or by increasing the out-of-plane rotation of y-branches with respect to the membrane.

Branched actin networks exhibit unique material properties distinct from those of isotropic actin gels

The elastic modulus of branched actin networks scales more weakly with density ($\sim c_A 0.6$) compared to isotropic gels ($\sim c_A 2$) and their response to test load ("pre-stress") does not follow a 'universal' scaling law. The stress-stiffening of isotropic actin networks has shown to be dominated by the entropy of individual filaments under tension (MacKintosh et al., 1995). Our data, however, indicate that the mechanics of anisotropic, branched actin networks assembled under load are determined by different microscopic processes. Instead of the entropic elasticity of long filaments, the higher stiffness and weaker dependence on density might reflect direct bending of short, stiff filaments constrained by the branched network architecture. Higher order phenomena, such as the interlocking of meso-scale arbors of branched filaments, may also contribute under these conditions. New theoretical approaches to actin mechanics will help resolve these questions.

Crosslinkers have different effects on branched actin network material properties

Differences in affinity and in network micro-architecture likely explain the differential effects of α-Actinin and Filamin A on sparse and dense branched actin networks. Filamin-A is a v-shape crosslinker that prefers actin filaments that cross orthogonally. α-Actinin, on the other hand, is a rod-shaped, anti-parallel dimer that can drive formation of gels or bundles. Under low load forces we suggest that the crossing angle between filaments from adjoining arbors will be ~72°, an angle determined by the geometry of Arp2/3-dependent branching and which favors binding of Filamin A. As the geometry of the network changes under load filaments from adjacent arbors intesect at higher angles, approaching 180° (anti-parallel), a configuration that disfavors Filamin A but not α-Actinin. This might explain why, at low growth forces the incorporation of α-Actinin has a modest effect compared to Filamin-A, while at high growth forces the effect of α-Actinin becomes more significant.

Motor activity of branched actin networks depends on loading history

Mechanical failure of actin networks may be an important element of their adaptation to mechanical loading. When the load on a growing network increases, newly formed material will be denser and stronger than older layers, which are crushed by the higher load forces. Plastic deformation of weaker layers reduces their contribution to the composite stiffness of the material and transiently reduces network expansion. Understanding the combined effects of force on assembly and mechanical collapse is essential to understanding how branched actin networks push against their cellular loads. Force-mediated coupling between filament assembly and material properties represents a key difference between the motor activity of branched networks and motor proteins such as myosin or kinesin. Under a given set of biochemical conditions, the activity of a motor protein is defined by a single force-velocity curve (Carter and Cross, 2005), whereas the motor activity of branched networks exhibits a spectrum of force-velocity relationships that depend on both the instantaneous internal stiffness of the network and the external stiffness of the material against which it pushes.

Experimental Procedures

Four main techniques are utilized in this paper: (1) reconstitution of branched networks from purified proteins (actin, profilin, Arp2/3, CP, and NPF), (2) biochemical surface micro-patterning of NPFs on coverslips, (3) atomic force microscopy to control the mechanical loading and to measure the material properties of the network, and (4) fluorescence microscopy (confocal, TIRF, and 3D STORM) of protein assembly in the network at bulk and single-molecule levels. After immersing the NPF patterned surface (technique 1) in assembly mix (5μM actin, 5μM profilin, 100nM Arp2/3, 100nM CP), branched networks grew (technique 2) under loads imposed by the AFM (technique 3) and molecular assembly was observed by fluorescence microscopy (technique 4). This experimental approach allowed us to quantify the effects of force on branched network growth. We simultaneously measured mechanical properties and fluorescence intensities of branched actin networks that were grown under biochemically and mechanically defined conditions. For complete experimental details, see Supplemental Materials and Methods.

Surface Micro-patterning

We coated the coverslip with a high density of diamino-polyethylene glycol (PEG), which was derivatized with maleimide. We then photo-eliminated maleimide groups in selected regions of the coverslip by UV irradiation through a photo mask, leaving square regions (14x14 μm^2 if not indicated otherwise) of intact maleimide. Unlike previous approaches (Reymann et al., 2010), our patterning method does not remove PEG molecules from the coverslip and therefore leaves the surface passivated. We reacted the intact maleimide regions with a WAVE1 mutant (WAVE1ΔN), which relplaced the N-terminal SH1 domain by mCherry and contained a single reactive cysteine residue at its N-terminus. This immobilizes the NPF in an oriented and mechanically stable manner.

Atomic Force Microscopy

To tightly couple the cantilevers to the network, we designed a custom cantilever holder to reduce the angle of the cantilever on glass substrate surface and coated cantilevers with a peptide from the filament-binding protein Ezrin. With these modifications, we never observed slippage between the cantilever and the network and, under loading conditions used in this study, we never observed the entire network macroscopically bend or buckle under the cantilever.

Supplementary Material

Refer to Web version on PubMed Central for supplementary material.

Acknowledgments

We thank Scott Hansen for reagents, discussions and comments on the manuscript, Thomas Surrey, Michael Vahey and Marcus Taylor for comments on the manuscript and members of the Fletcher and Mullins labs for discussions. This work was supported by NIH R01 GM074751 (D.A.F.), NIH R01 GM061010 (R.D.M), HHMI (R.D.M.). HFSP LT-000843/2010 (P.B), EMBO ALTF 854-2009 (P.B). T.-D.L. was supported by the Taiwan National Science Council.

References

Akin O, Mullins RD. Capping protein increases the rate of actin-based motility by promoting filament nucleation by the Arp2/3 complex. Cell. 2008; 133:841–851. [PubMed: 18510928]

Beltzner CC, Pollard TD. Pathway of actin filament branch formation by Arp2/3 complex. J Biol Chem. 2008; 283:7135–7144. [PubMed: 18165685]

Bisi S, Disanza A, Malinverno C, Frittoli E, Palamidessi A, Scita G. Membrane and actin dynamics interplay at lamellipodia leading edge. Curr Opin Cell Biol. 2013; 25:565–573. [PubMed: 23639310]

Cameron LA, Svitkina TM, Vignjevic D, Theriot JA, Borisy GG. Dendritic organization of actin comet tails. Curr Biol. 2001; 11:130–135. [PubMed: 11231131]

Carter NJ, Cross RA. Mechanics of the kinesin step. Nature. 2005; 435:308–312. [PubMed: 15902249]

Chaudhuri O, Parekh SH, Fletcher DA. Reversible stress softening of actin networks. Nature. 2007; 445:295–298. [PubMed: 17230186]

Clark AG, Miller AL, Vaughan E, Yu HYE, Penkert R, Bement WM. Integration of single and multicellular wound responses. Curr Biol. 2009; 19:1389–1395. [PubMed: 19631537]

Flanagan LA, Chou J, Falet H, Neujahr R, Hartwig JH, Stossel TP. Filamin A, the Arp2/3 complex, and the morphology and function of cortical actin filaments in human melanoma cells. J Cell Biol. 2001; 155:511–517. [PubMed: 11706047]

Fletcher DA, Mullins RD. Cell mechanics and the cytoskeleton. Nature. 2010; 463:485–492. [PubMed: 20110992]

Fourniol FJ, Li TD, Bieling P, Mullins RD, Fletcher DA, Surrey T. Micropattern-guided assembly of overlapping pairs of dynamic microtubules. Meth Enzymol. 2014; 540:339–360. [PubMed: 24630116]

Gardel ML, Valentine MT, Crocker JC, Bausch AR, Weitz DA. Microrheology of entangled F-actin solutions. Phys Rev Lett. 2003; 91:158302. [PubMed: 14611506]

Gardel ML, Shin JH, MacKintosh FC, Mahadevan L, Matsudaira P, Weitz DA. Elastic behavior of cross-linked and bundled actin networks. Science. 2004a; 304:1301–1305. [PubMed: 15166374]

Gardel ML, Shin JH, MacKintosh FC, Mahadevan L, Matsudaira PA, Weitz DA. Scaling of F-actin network rheology to probe single filament elasticity and dynamics. Phys Rev Lett. 2004b; 93:188102. [PubMed: 15525211]

Gardel ML, Nakamura F, Hartwig JH, Crocker JC, Stossel TP, Weitz DA. Prestressed F-actin networks cross-linked by hinged filamins replicate mechanical properties of cells. Proc Natl Acad Sci USA. 2006; 103:1762–1767. [PubMed: 16446458]

Gardel ML, Sabass B, Ji L, Danuser G, Schwarz US, Waterman CM. Traction stress in focal adhesions correlates biphasically with actin retrograde flow speed. J Cell Biol. 2008; 183:999–1005. [PubMed: 19075110]

Hill TL, Kirschner MW. Bioenergetics and kinetics of microtubule and actin filament assembly-disassembly. Int Rev Cytol. 1982; 78:1–125. [PubMed: 6128332]

Huang B, Wang W, Bates M, Zhuang X. Three-dimensional super-resolution imaging by stochastic optical reconstruction microscopy. Science. 2008; 319:810–813. [PubMed: 18174397]

Insall RH, Machesky LM. Actin dynamics at the leading edge: from simple machinery to complex networks. Dev Cell. 2009; 17:310–322. [PubMed: 19758556]

Janmey PA, McCulloch CA. Cell mechanics: integrating cell responses to mechanical stimuli. Annu Rev Biomed Eng. 2007; 9:1–34. [PubMed: 17461730]

Janmey PA, Euteneuer U, Traub P, Schliwa M. Viscoelastic properties of vimentin compared with other filamentous biopolymer networks. J Cell Biol. 1991; 113:155–160. [PubMed: 2007620]

Kasza KE, Rowat AC, Liu J, Angelini TE, Brangwynne CP, Koenderink GH, Weitz DA. The cell as a material. Curr Opin Cell Biol. 2007; 19:101–107. [PubMed: 17174543]

MacKintosh, Käs, Janmey. Elasticity of semiflexible biopolymer networks. Phys Rev Lett. 1995; 75:4425–4428. [PubMed: 10059905]

Maly IV, Borisy GG. Self-organization of a propulsive actin network as an evolutionary process. Proc Natl Acad Sci USA. 2001; 98:11324–11329. [PubMed: 11572984]

Marcy Y, Prost J, Carlier MF, Sykes C. Forces generated during actin-based propulsion: a direct measurement by micromanipulation. Proc Natl Acad Sci USA. 2004; 101:5992–5997. [PubMed: 15079054]

Mogilner A, Oster G. Cell motility driven by actin polymerization. Biophys J. 1996; 71:3030–3045. [PubMed: 8968574]

Mooren OL, Galletta BJ, Cooper JA. Roles for actin assembly in endocytosis. Annu Rev Biochem. 2012; 81:661–686. [PubMed: 22663081]

Mullins RD, Heuser JA, Pollard TD. The interaction of Arp2/3 complex with actin: nucleation, high affinity pointed end capping, and formation of branching networks of filaments. Proc Natl Acad Sci USA. 1998; 95:6181–6186. [PubMed: 9600938]

Nakamura F, Osborn E, Janmey PA, Stossel TP. Comparison of filamin A-induced cross-linking and Arp2/3 complex-mediated branching on the mechanics of actin filaments. J Biol Chem. 2002; 277:9148–9154. [PubMed: 11786548]

Nakamura F, Osborn TM, Hartemink CA, Hartwig JH, Stossel TP. Structural basis of filamin A functions. J Cell Biol. 2007; 179:1011–1025. [PubMed: 18056414]

Pantaloni D, Carlier MF. How profilin promotes actin filament assembly in the presence of thymosin beta 4. Cell. 1993; 75:1007–1014. [PubMed: 8252614]

Parekh SH, Chaudhuri O, Theriot JA, Fletcher DA. Loading history determines the velocity of actin-network growth. Nat Cell Biol. 2005; 7:1219–1223. [PubMed: 16299496]

Peskin CS, Odell GM, Oster GF. Cellular motions and thermal fluctuations: the Brownian ratchet. Biophys J. 1993; 65:316–324. [PubMed: 8369439]

Pollard TD, Cooper JA. Actin, a central player in cell shape and movement. Science. 2009; 326:1208–1212. [PubMed: 19965462]

Prass M, Jacobson K, Mogilner A, Radmacher M. Direct measurement of the lamellipodial protrusive force in a migrating cell. J Cell Biol. 2006; 174:767–772. [PubMed: 16966418]

Pujol T, du Roure O, Fermigier M, Heuvingh J. Impact of branching on the elasticity of actin networks. Proc Natl Acad Sci USA. 2012; 109:10364–10369. [PubMed: 22689953]

Renkawitz J, Schumann K, Weber M, Lämmermann T, Pflicke H, Piel M, Polleux J, Spatz JP, Sixt M. Adaptive force transmission in amoeboid cell migration. Nat Cell Biol. 2009; 11:1438–1443. [PubMed: 19915557]

Reymann AC, Martiel JL, Cambier T, Blanchoin L, Boujemaa-Paterski R, Théry M. Nucleation geometry governs ordered actin networks structures. Nat Mater. 2010; 9:827–832. [PubMed: 20852617]

Reymann AC, Suarez C, Guérin C, Martiel JL, Staiger CJ, Blanchoin L, Boujemaa-Paterski R. Turnover of branched actin filament networks by stochastic fragmentation with ADF/cofilin. Mol Biol Cell. 2011; 22:2541–2550. [PubMed: 21613547]

Schafer DA, Jennings PB, Cooper JA. Dynamics of capping protein and actin assembly in vitro: uncapping barbed ends by polyphosphoinositides. J Cell Biol. 1996; 135:169–179. [PubMed: 8858171]

Schaus TE, Taylor EW, Borisy GG. Self-organization of actin filament orientation in the dendritic-nucleation/array-treadmilling model. Proc Natl Acad Sci USA. 2007; 104:7086–7091. [PubMed: 17440042]

Storm C, Pastore JJ, MacKintosh FC, Lubensky TC, Janmey PA. Nonlinear elasticity in biological gels. Nature. 2005; 435:191–194. [PubMed: 15889088]

Stricker J, Falzone T, Gardel ML. Mechanics of the F-actin cytoskeleton. J Biomech. 2010; 43:9–14. [PubMed: 19913792]

Svitkina TM, Borisy GG. Arp2/3 complex and actin depolymerizing factor/cofilin in dendritic organization and treadmilling of actin filament array in lamellipodia. J Cell Biol. 1999; 145:1009–1026. [PubMed: 10352018]

Tilney LG, Bonder EM, Coluccio LM, Mooseker MS. Actin from Thyone sperm assembles on only one end of an actin filament: a behavior regulated by profilin. J Cell Biol. 1983; 97:112–124. [PubMed: 6863386]

Vinzenz M, Nemethova M, Schur F, Mueller J, Narita A, Urban E, Winkler C, Schmeiser C, Koestler SA, Rottner K, et al. Actin branching in the initiation and maintenance of lamellipodia. J Cell Sci. 2012; 125:2775–2785. [PubMed: 22431015]

Wachsstock DH, Schwartz WH, Pollard TD. Affinity of alpha-actinin for actin determines the structure and mechanical properties of actin filament gels. Biophys J. 1993; 65:205–214. [PubMed: 8369430]

Wagner B, Tharmann R, Haase I, Fischer M, Bausch AR. Cytoskeletal polymer networks: the molecular structure of cross-linkers determines macroscopic properties. Proc Natl Acad Sci USA. 2006; 103:13974–13978. [PubMed: 16963567]

Weichsel J, Urban E, Small JV, Schwarz US. Reconstructing the orientation distribution of actin filaments in the lamellipodium of migrating keratocytes from electron microscopy tomography data. Cytometry A. 2012; 81:496–507. [PubMed: 22499256]

Welch MD, Way M. Arp2/3-mediated actin-based motility: a tail of pathogen abuse. Cell Host Microbe. 2013; 14:242–255. [PubMed: 24034611]

Wu C, Asokan SB, Berginski ME, Haynes EM, Sharpless NE, Griffith JD, Gomez SM, Bear JE. Arp2/3 is critical for lamellipodia and response to extracellular matrix cues but is dispensable for chemotaxis. Cell. 2012; 148:973–987. [PubMed: 22385962]

Yamaguchi H, Lorenz M, Kempiak S, Sarmiento C, Coniglio S, Symons M, Segall J, Eddy R, Miki H, Takenawa T, et al. Molecular mechanisms of invadopodium formation: the role of the N-WASP-Arp2/3 complex pathway and cofilin. J Cell Biol. 2005; 168:441–452. [PubMed: 15684033]

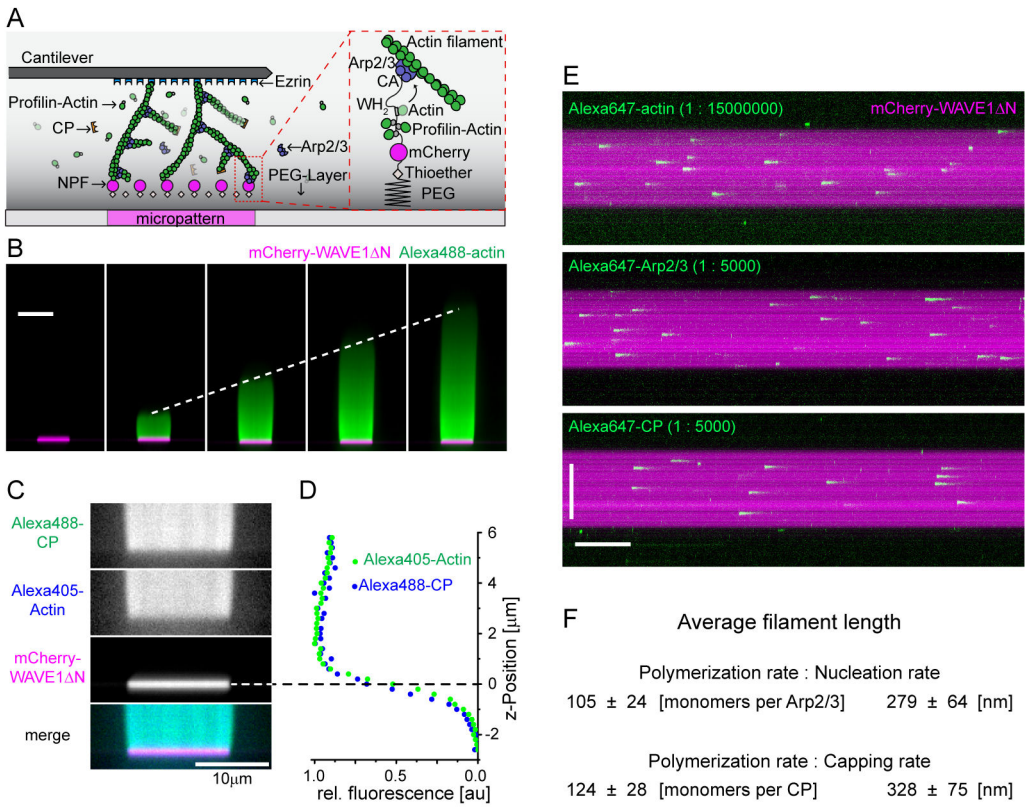

Fig. 1. Reconstitution of branched network with in vivo-like properties from micropatterned surfaces

(A) Scheme: NPF patches, bound to a PEG passivated coverslip, rapidly assemble dendritic networks from profilin-actin, CP and Arp2/3. Networks are visualized by fluorescence microscopy and mechanically manipulated through an AFM cantilever. **(B)** Confocal microscopy (reconstructed axial view) of actin assembly (Alexa488-actin, green) from WAVE1ΔN micropatterns (magenta) after indicated time of protein addition (5μM actin (1% Alexa 488-labeled), 5μM profilin, 100nM Arp2/3, 100nM CP). **(C)** Reconstructed axial view for indicated dendritic network components from confocal imaging. Conditions as in B) with 15% TMR-CP and 5% Alexa647-Arp2/3. **(D)** Intensity profiles of actin (blue) and CP (green) along axial dimension from confocal microscopy. Surface position (z=0) was defined by the maximal mCherry-WAVE1 fluorescence signal (dashed line) **(E)** Space-time plots (kymographs) from single molecule TIRF imaging of either actin (top), Arp2/3 (middle) or CP (bottom) incorporation into dendritic networks at a small reference stress of 25 pN/μm^2. Rates were determined by the product of the incorporation rate and the known labeling ratio (see Suppl. Methods). **(F)** Average filament lengths as determined by the ratio of the single-molecule polymerization and the nucleation (top) or the capping (bottom) rate. All error indicators are SEM.

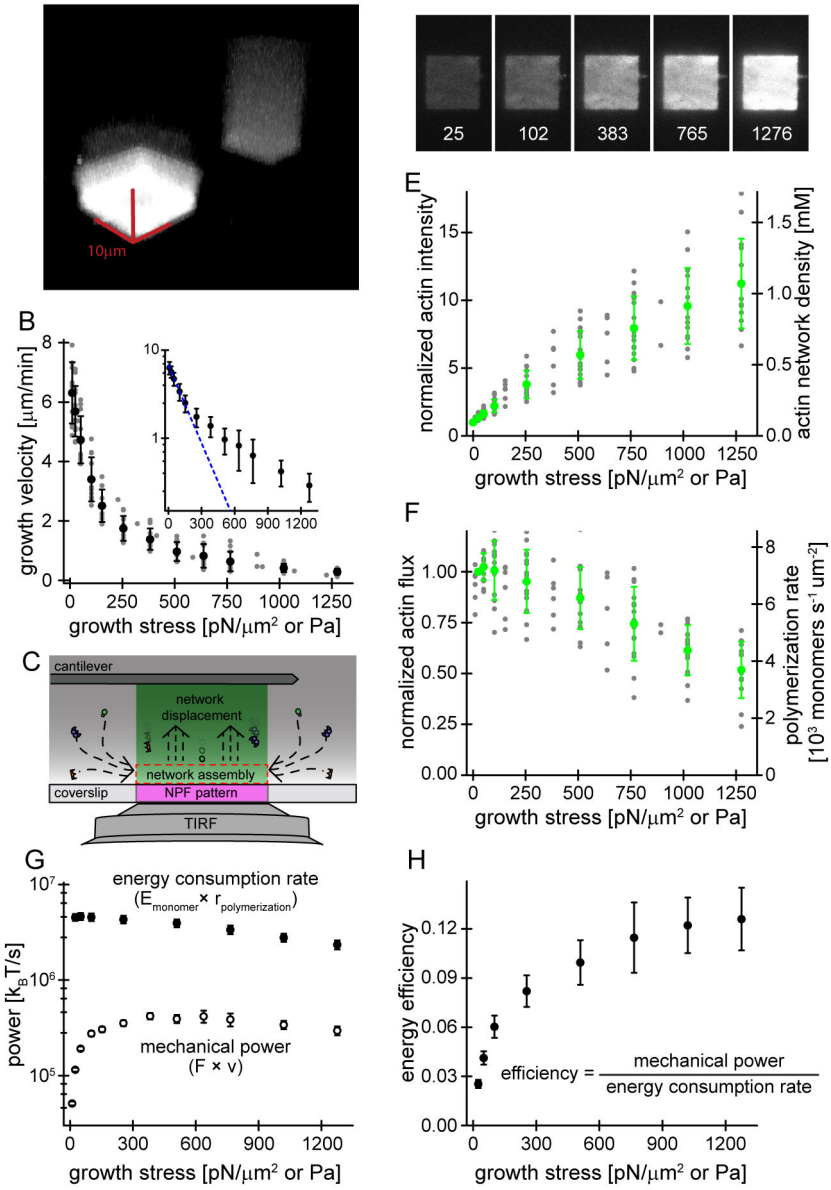

Fig. 2. Force-feedback increases density and mechanical efficiency of branched actin networks

(A) 3D reconstruction from confocal microscopy of two networks growing under an AFM cantilever (left) or freely into solution (right). **(B)** Steady-state growth velocities of networks as a function of growth stress. Grey=raw data, black=averages. Inset is a semi-logarithmic replot together with a single exponential fit (dashed blue line) to the low-force data. **(C)** Scheme of network assembly visualized by TIRFM. **(D)** TIRFM images of networks (Alexa488-actin) at indicated growth stress. **(E)** Actin intensity (left y-axis, normalized to unloaded control) and the calculated actin density (right y-axis, calibrated by single molecule experiments (Fig. 1E and Methods)) as a function of growth stress. Grey=raw data, green=averages. **(F)** Actin flux (left y-axis, product of network density (see Fig. 2B) and growth velocity (see Fig. 2C), normalized to flux at 25 pN/µm^2) and polymerization rates (right y-axis, calibrated by single molecule experiments (see Fig.1E)) as a function of

growth stress. Grey=raw data, green=averages. **(G)** Logarithmic plot of energy consumption rate (product of polymerization rate ($r_{polymerization}$, Fig. 2F) and free energy change per monomer ($E_{monomer}$= 3.18 k_BT, see Suppl. Methods)) and mechanical power (calculated by the product of velocity (v) and force (F) (see Fig. 2E)) as a function of growth stress. **(H)** Mean energy efficiency (determined by the ratio of the mechanical power and the energy consumption rate (see Fig. 2G)) as a function of growth stress. Error bars are SD (B, E, F) or SEM (G,H).

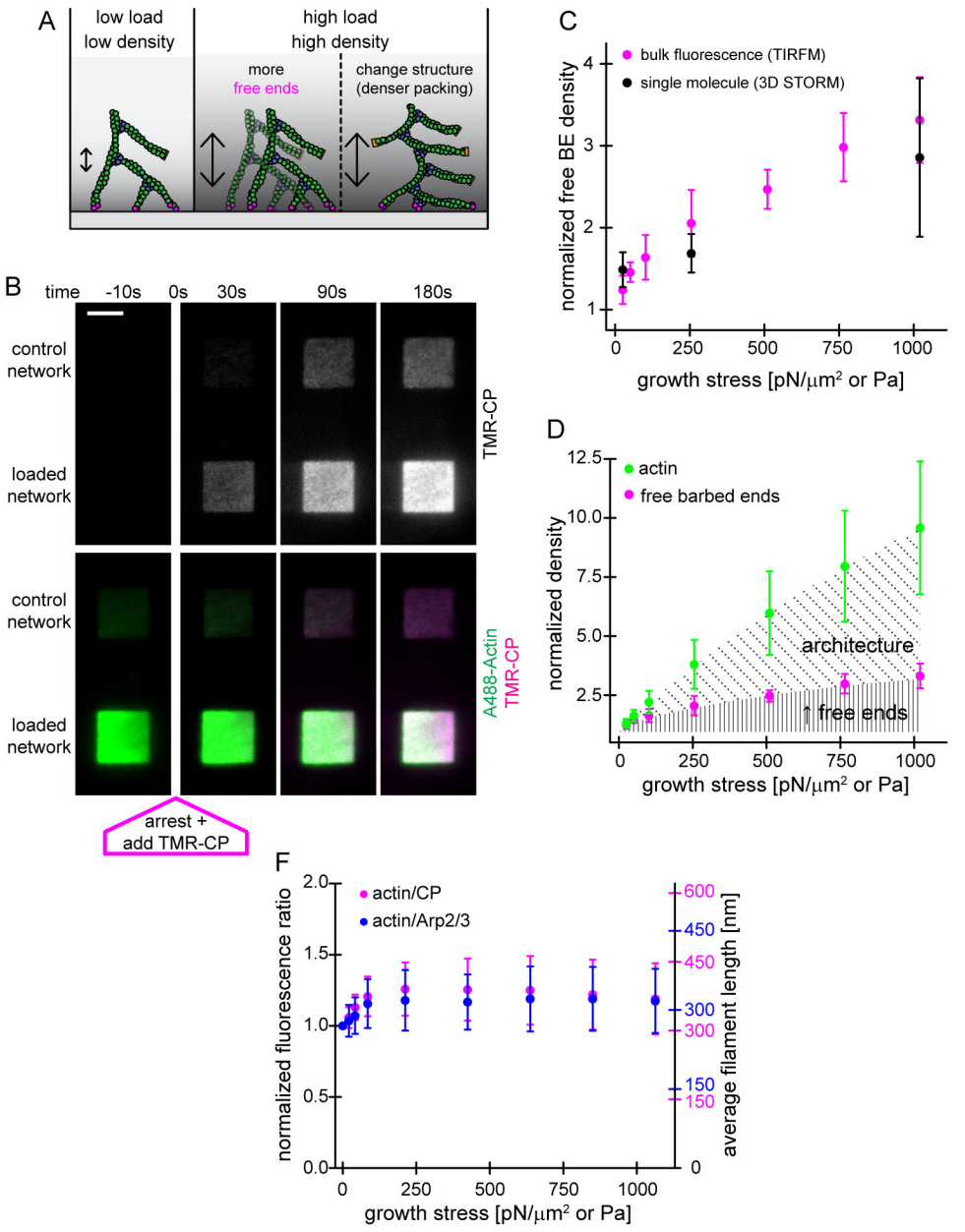

Fig. 3. Force-feedback increases the density of free barbed ends within the network but does not alter the stoichiometry of its constituents

(A) Scheme of network assembly under low (left) or high stress (middle and right). Density increase by either rise in the number of free ends (middle) and/or changes in packing of filaments (right). **(B)** TIRFM images of TMR-CP binding (top alone (greyscale) or as color merge with Alexa488-actin (green and magenta, bottom)) to networks either unloaded or assembled under 1020 pN/μm^2 load at indicated times after kinetic arrest (t=0 is the addition of labeling mix (27.5 μM Latrunculin B, 27.5μM phalloidin, 18.5 nM TMR-CP). **(C)** Free barbed end densities (normalized to unloaded control) from either TIRFM (magenta) or 3D STORM (black) as a function of growth stress. **(D)** Free barbed end (magenta) or actin (green) densities normalized to unloaded control as a function of growth stress. The

increased free end density (vertical, solid lines) accounts for a fraction of actin density rise and the residual rise is due to denser filament packing (diagonal, dotted lines). **(E)** Ratio of fluorescence intensities (left y-axis, normalized to unloaded control) or average filament lengths (right y-axis, calibrated by single molecule assays, Fig.1F) of actin/CP (magenta) or actin/Arp2/3 (blue) as a function of growth stress. Error bars are SD.

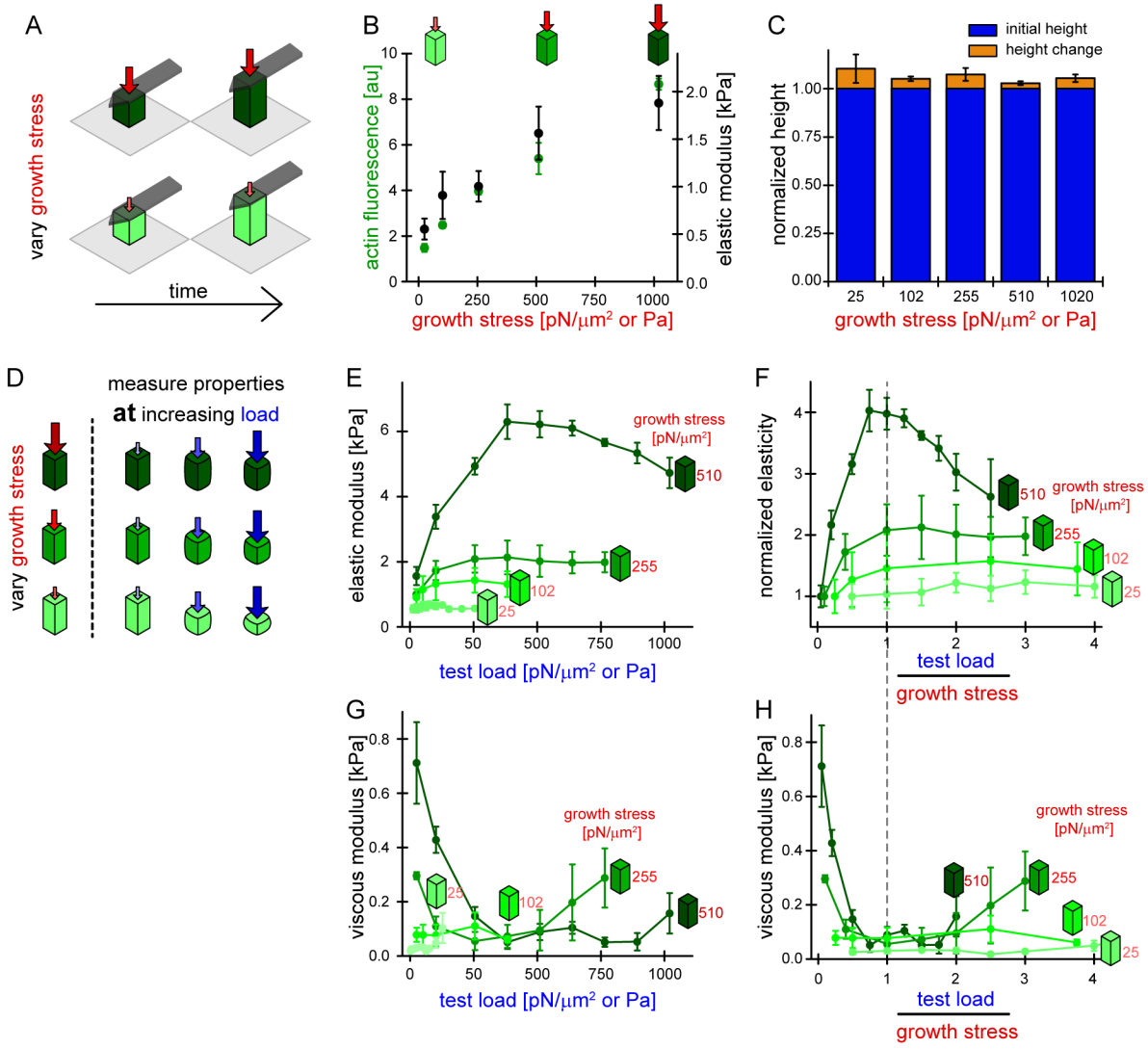

Fig. 4. Adaptation to load- and growth-forces shapes the material properties of branched networks

(A) Scheme of network assembly under high (dark red arrow, top) or low (light red arrow, bottom) growth stress, resulting in high (dark green) or low (light green) network density. **(B)** Actin fluorescence from TIRFM imaging (green, left y-axis) and initial elasticity from microrheology (black, right y-axis) as a function of growth stress. Measurements were performed at low test load (12.5–25 pN/μm^2) following network arrest. **(C)** Change in network height (orange) after growth stress release to low levels (12.5 - 25 pN/μm^2) following arrest for networks assembled at different growth stresses as indicated. Height was normalized to the initial network height at the moment of growth arrest (blue). **(D)** Scheme: Networks are assembled under growth stresses (red arrows, left), arrested (dashed line) and then subjected to increasing test load (blue arrows, right). Elasticity is measured at each test load. **(E)** Network elasticity as a function of test load for networks assembled at different growth stresses as indicated. **(F)** as (E) with elasticity normalized to the initial elasticity and the test load normalized to the growth stress. **(G)** Network viscosity as a function of test load

for networks assembled under different growth stresses as indicated. **(H)** Same as (G) but with the test load normalized to the growth stress. Error bars are SD (B–C) or are ½ SD (D–H).

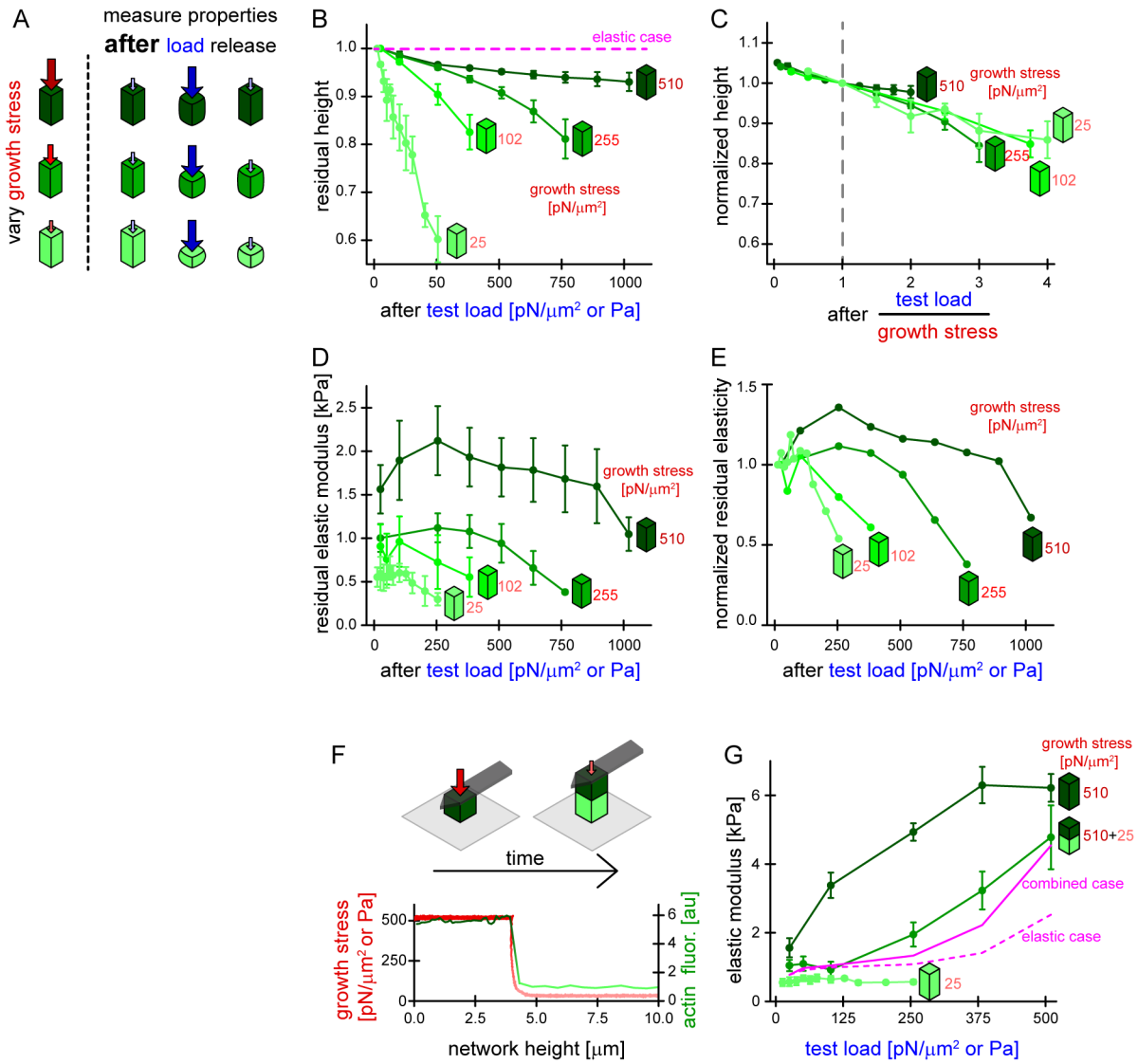

Fig. 5. Loading beyond the growth force causes mechanical failure leading to history-dependent mechanical properties

(A) Scheme: Networks are assembled at different growth stresses (red arrow, left) resulting in different network densities (green), arrested (dashed line) and initial height and elasticity are measured under low test load. Networks are then subjected to stress cycles consisting of high test load followed by a low test load, recovery step during which the residual height and elasticity is determined (blue arrows, right). **(B)** Residual network height (normalized to the initial height) measured during the recovery step as a function of the previously applied high test load for networks assembled under different growth stress. The dashed magenta line is the ideal elastic case (full recovery). **(C)** Same as (B) but with the test load normalized to the growth stress. Residual network height was normalized to the residual height after the test load reached the growth stress. **(D)** Residual network elasticity measured during the recovery step as a function of the previously applied high test load for networks assembled under different growth stresses. **(E)** Same as (D) but with the residual elasticity normalized

to the initial elasticity. **(F)** Top: Composite network assembly. Networks are first assembled at a high growth stress, i.e at high actin density (left). Upon reaching a defined height, growth stress is reduced giving rise to a sparse network layer (right). Bottom: Growth stress (red, left y-axis) and actin fluorescence (green, right y-axis) of a discontinuous, two-layered network as a function of network height. **(G)** Network elasticity as a function of test load for either homogenous networks assembled at constant growth stress (510 or 25 pN/μm^2) or a composite network assembled at 510 and 25 pN/μm^2 as indicated. Dashed magenta line is the estimated network elasticity for the composite network assuming purely elastic behavior (Methods). The continuous magenta line is an estimate that additionally includes mechanical failure (plastic deformation) (Methods). All error bars are ½ SD.

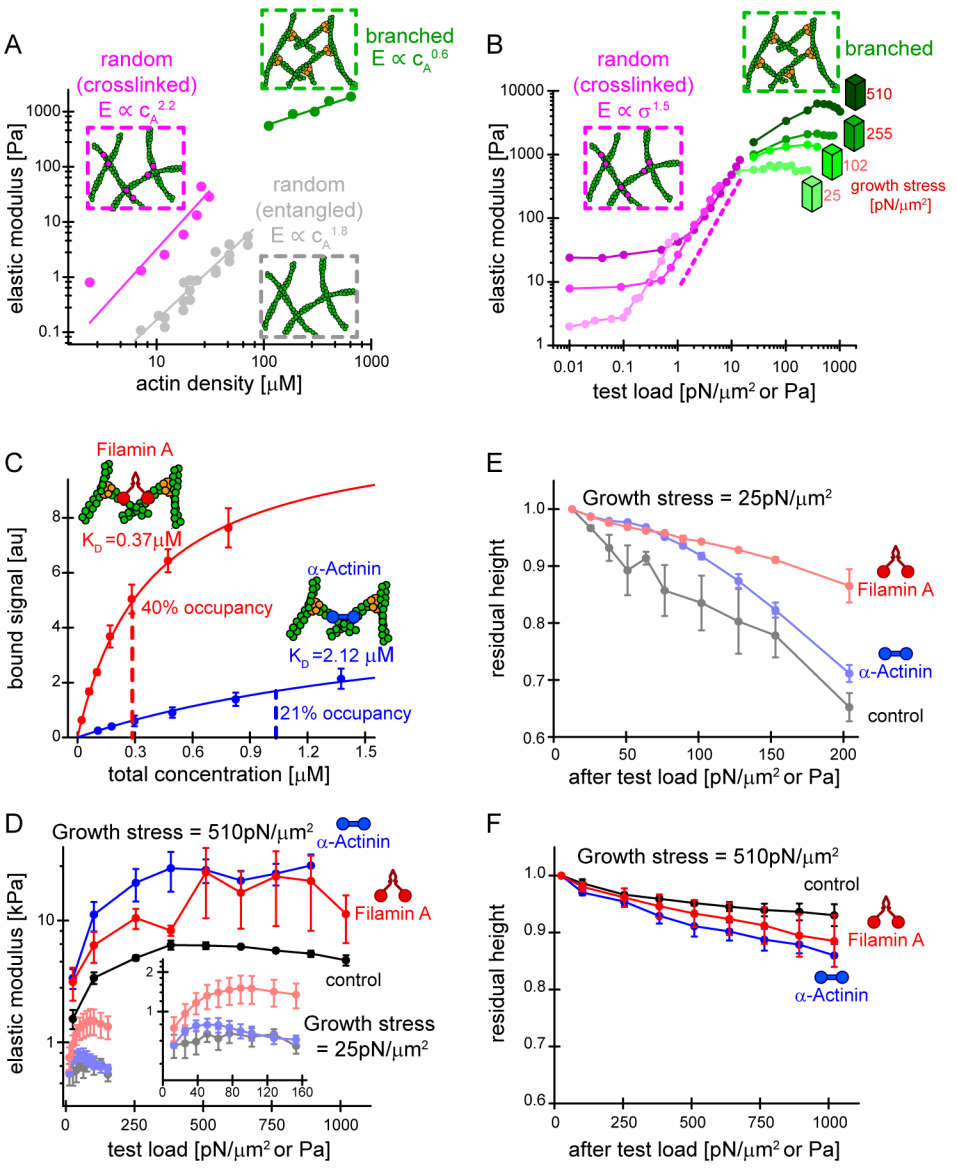

Fig. 6. Branched network mechanics are distinct from random gels and not fundamentally changed by crosslinkers

(A) Elasticity of entangled (light grey, from Gardel et al., 2003) or cross-linked random gels (dark grey, from Gardel et al., 2004, 0.03 actin:scruin ratio) compared to branched networks (green) as a function of actin density. Lines are power laws with indicated scaling factors (Methods). **(B)** Double-logarithmic plot of network elasticity as a function of test load (prestress) for either random cross-linked networks of different actin concentration (magenta, from dark to light=29.4, 21.4, 8.33 μM, 0.03 actin:scruin ratio, from Gardel et al., 2004) or branched networks assembled at indicated growth stress (green). The dashed magenta line indicates the “universal” scaling behavior of random actin gels. **(C)** Fluorescence of network-bound Filamin-A (red) or a-Actinin (blue) by confocal microscopy as a function of total concentration. Lines are fits to single-site binding models. Dashed lines indicate concentrations used for mechanical measurements resulting in a fractional

occupancy of binding sites as indicated **(D)** Network elasticity as a function of test load for networks assembled at a growth stress of 25 (light) or 510 pN/μm^2 (dark) growth stress and additionally crosslinked with either Filamin-A (red) or a-Actinin (blue) or a buffer control (black). **(E)** Residual network height (normalized to initial network height) for networks assembled at low (25 pN/μm^2) growth stress, crosslinked with Filamin-A (red), α-Actinin (blue) or a buffer control (black) as a function of the previously applied test load. Height was measured during the recovery step. **(F)** Same as (E) but for networks assembled at high (510 pN/μm^2) growth stress. All error bars are ½ SD.

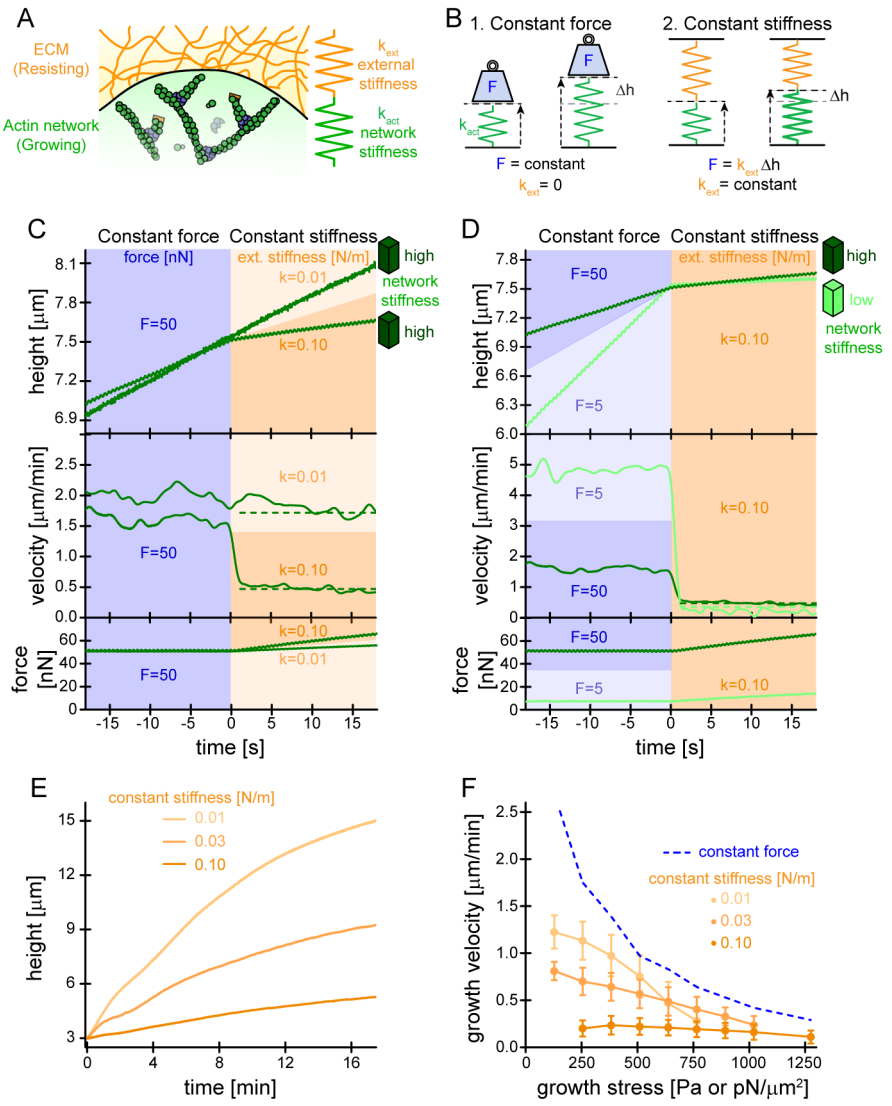

Fig. 7. Branched network motor activity depends on the mechanical environment

(A) Scheme of branched actin networks (green) pushing against the ECM (orange) at the leading edge. **(B)** Scheme of a network pushing against an AFM cantilever. The AFM can operate either keeping the force constant (zero external stiffness, left) or the external stiffness constant (defined force at a given cantilever deflection, right). **(C)** Sample height (top), normalized growth velocity (middle) and force (bottom) for two networks assembled under constant high (50 nN) growth force (blue area), resulting in high (dark green traces) network stiffness. At t=0, force-feedback is disengaged and networks displace cantilevers imposing either high (k=0.1N/m, dark orange area) or low (k=0.01N/m, light orange area) external stiffness. The drop in velocity can be predicted (dashed lines) from the known network stiffness (Methods). **(D)** Same as (C) for two networks grown under constant high (50 nN, dark blue area) or low (5 nN, light blue area) growth force (light blue area), resulting in high (dark green trace) and low (light green trace) network stiffness, respectively. After disengaging the force-feedback, networks are challenged with the same

external cantilever stiffness (k=0.1 N/m, dark orange area) **(E)** Sample height as a function of time for networks pushing against cantilevers of different stiffnesses. Networks were grown in the absence of force to a height of 3μm before cantilever contact (t=0). **(F)** Network growth velocity as a function of growth force under either constant force (blue dashed line, see Fig. 2E) or constant stiffness conditions (orange) for three different external (cantilever) stiffnesses as indicated. Error bars are SD.